Materials Science and Engineering A 395 (2005) 269–280

www.elsevier.com/locate/msea

Enhanced ductility in thermally sprayed titania coating synthesized using a nanostructured feedstock

R.S. Lima *, B.R. Marple

National Research Council of Canada, 75 de Mortagne Blvd., Boucherville, QC J4B 6Y4, Canada

Received 12 October 2004; accepted 17 December 2004

Abstract

Nanostructured and conventional titania (TiO_2) feedstock powders were thermally sprayed via high velocity oxy-fuel (HVOF). The microstructure, porosity, Vickers hardness, crack propagation resistance, bond strength (ASTM C633), abrasion behavior (ASTM G65) and the wear scar characteristics of these two types of coatings were analyzed and compared. The coating made from the nanostructured feedstock exhibited a bimodal microstructure, with regions containing particles that were fully molten (conventional matrix) and regions with embedded particles that were semi-molten (nanostructured zones) during the thermal spraying process. The bimodal coating also exhibited higher bond strength and higher wear resistance when compared to the conventional coating. By comparing the wear scars of both coatings (via scanning electron microscopy and roughness measurements) it was observed that when the coatings were subjected to the same abrasive conditions the wear scar of the bimodal coating was smoother, with more plastically deformed regions than the conventional coating. It was concluded that this enhanced ductility of the bimodal coating was caused by its higher toughness. The results suggest that nanostructured zones randomly distributed in the microstructure of the bimodal coating act as crack arresters, thereby enhancing toughness and promoting higher critical depth of cut, which provides a broader plastic deformation range than that exhibited by the conventional coating. This work provides evidence that the enhanced ductility of the bimodal coating is a nanostructured-related property, not caused by any other microstructural artifact.

Keywords: Thermal spray; Titania (TiO_2); Nanostructure; Ductility; Abrasion resistance; Bond strength

1. Introduction

1.1. Ductility in nanostructured materials

Ductility is defined as the ability of a material to change shape without fracture. It is of critical importance during the processing of materials. Usually it is considered that materials may be strong or ductile, but rarely both at once. However, from a phenomenological point of view, nanostructured materials may exhibit both characteristics. Nanostructured materials have structural features, such as grain sizes, that are less than 100 nm in dimension [1]. The Hall-Petch empirical relationship points to the potential of improving the mechanical properties of materials when decreasing the grain size [2]. In terms of yield strength and hardness, the expressions are:

$$\sigma_y = \sigma_0 + kd^{-1/2} \quad (1)$$

$$H = H_0 + k'd^{-1/2} \quad (2)$$

where σ_y and H refer to the yield strength and hardness of the material, respectively, the subscript 0 relating to the material's infinite grain size; k and k' are constants representing the grain boundary as an obstacle to the propagation of deformation (metal) or crack (ceramics); and d is grain size.

Superplastic behavior, which is defined as the ability of a crystalline material to undergo large elongations (on the order of hundreds or thousands of percent) prior to failure, can also be related to the material's grain size [3,4]. The equation is

* Corresponding author. Tel.: +1 450 641 5150; fax: +1 450 641 5105.
E-mail address: rogerio.lima@cnrc-nrc.gc.ca (R.S. Lima).

0921-5093/$ – see front matter.
doi:10.1016/j.msea.2004.12.039

given by:

$$\dot{\varepsilon} = A\frac{\sigma^n}{d^p}\exp\left(-\frac{Q}{RT}\right) \quad (3)$$

where $\dot{\varepsilon}$ is the strain rate, A is a constant, σ is the stress, n is the stress exponent, d is the grain size, p is the grain size exponent, Q is the activation energy, R is the gas constant and T is the temperature.

Eqs. (1)–(3) show that when reducing grain sizes from conventional levels (i.e., <10 μm in metals and <1–2 μm in ceramics) to nanostructured levels (i.e., <100 nm) the mechanical strength and ductility of materials can be considerably enhanced.

It has been demonstrated that nanostructured metals, in some cases, may exhibit high strength while maintaining very good ductility [5]. The mechanisms by which high strength and ductility coexist in metals are still under discussion and it is not yet clear what particular microstructures or deformation mechanisms are responsible for the good ductility [5–8]. A new approach for high strength–high ductility materials was given by Wang et al. [9]. In that work a nanostructured copper was produced by rolling the metal at liquid nitrogen temperature and heating it to around 180 °C. The result was a bimodal structure of micron-sized grains embedded in a matrix of nano-sized material. The material exhibited high strength and retained its high ductility. It was believed that the nano-sized grains provided strength, whereas the embedded large grains stabilized the tensile deformation of the material [9]. Despite this observed enhanced ductility in some nanostructured metals, there has been no evidence of superplasticity at room temperature.

High ductility at low temperatures in nanostructured ceramic materials is a subject that has generated considerable debate in the scientific community. Mayo et al. [10] showed by using indentation techniques that nanostructured titania exhibited higher ductility at room temperature when compared to a conventional sample. However, the nanostructured titania sample employed was not fully dense, whereas the conventional sample was a dense single crystal. Plastic deformation and toughness results from indentation tests performed on porous samples may be of questionable value. Porosity may allow materials to appear to deform plastically underneath an indenter, when in fact the material is merely densifying by the fracture, rearrangement and sliding of particles into the pores [11–14]. A porous material showing this "apparent ductility" would not necessarily exhibit low temperature plasticity or high toughness in the fully dense state. In order to measure meaningful ductility values in nanostructured materials, near pore-free samples are required [13].

Cottom and Mayo [11] employed nanostructured and conventional samples of ZrO_2–Y_2O_3 for fracture toughness measurements via Vickers indentation. The samples exhibited densities higher than 90% of the theoretical density. The results implied that there was not a significant room temperature ductility mechanism peculiar to the nanostructured ceramic material. Mayo [14] arrived at the same conclusion with TiO_2 and ZnO. Therefore the predicted enhanced ductility in nanostructured ceramics at temperatures significantly lower than $0.5T_m$ has not been achieved.

1.2. Nanostructured ceramics and thermal spray coatings

In addition to bulk samples, the study of nanostructured ceramics has been extended to coatings processed using the thermal spray technique [15–18]. During the thermal spraying of ceramics using the traditional approach it is necessary to melt the powder particles in order to achieve the necessary physical conditions for coating formation, i.e., the cohesion and adhesion of the thermally sprayed particles on the substrate surface. If nanostructured powder particles are fully melted during thermal spraying, any nanostructured-based property of the feedstock is lost. Therefore it is paramount to engineer thermal spray parameters (i.e., distributions of particle temperature and velocity in the thermal spray jet) that allow partial melting of the powder particles during spraying. The particles that were fully molten in the thermal spray jet will surround the semi-molten particles during coating formation, thereby maintaining coating integrity. For this reason the microstructures of ceramic thermal spray coatings made from nanostructured ceramic powders exhibit a bimodal distribution [15–18]. The semi-molten nanostructured particles (nanostructured zones) are embedded in the conventional matrix formed by the particles that were fully molten in the thermal spray jet.

Different authors [17–20] have demonstrated that thermally sprayed coatings made from nanostructured ceramic feedstock powders exhibit superior wear resistance when compared to conventional counterparts. Using indentation techniques it was found that the coatings made from nanostructured powders exhibited higher crack propagation/growth resistance or relative toughness when compared to the conventional coatings [17,18,20]. It was observed that the semi-molten particles (nanostructured zones) in the bimodal coatings acted as crack arresters, enhancing coating toughness and thereby increasing wear resistance. These findings led to one of the first attempts of "real world" utilization of nanostructured-related materials in structural applications [17,19].

Although higher toughness was observed for the bimodal coatings, consideration was not given to the possibility of the existence of an enhanced ductility at room temperature. Gell et al. [17] observed that the wear scars of the bimodal coatings were smoother than those of the conventional coatings, however, further considerations on a supposed higher ductility of the bimodal coatings were not sought.

In the present work, nanostructured and conventional titania feedstock powders were thermally sprayed. The objective was to produce coatings with some key spraying and microstructural similarities, such as, similar distribution of particle temperature and velocity in the thermal spray jet, highly

dense coatings (porosity <1%) and similar phase composition. It was believed that if these similarities were achieved, a fair comparison of the mechanical performance of the two materials could be made, and even a possible enhanced ductility at low temperatures for the bimodal coating could be considered (if present) and observed.

2. Experimental procedure

2.1. Feedstocks

Nanostructured and conventional titania (TiO_2) feedstock powders were employed in this work. The nanostructured titania feedstock (VHP-DCS (5–20 μm), Altair Nanomaterials Inc., Reno, NV, USA) was (according to the manufacturer) agglomerated and sintered and exhibited a nominal particle size range from 5 to 20 μm. The conventional titania feedstock (Flomaster 22.8(99)F4, F.J. Brodmann and Co., Harvey, LA, USA) was (according to the manufacturer) fused and crushed and had a nominal particle size range from 5 to 20 μm.

2.2. Thermal spraying and in-flight particle diagnostics

The two feedstock powders were thermally sprayed via the high velocity oxy-fuel (HVOF) technique using an oxy-propylene based HVOF torch (Diamond Jet 2700-hybrid, Sulzer Metco, Westbury, NY, USA). The coatings were deposited on low carbon steel substrates that had been grit-blasted to roughen the surface before spraying. Initially during HVOF spraying, various O_2/propylene flow ratios were tested by monitoring particle temperature and velocity using a diagnostic tool (DPV 2000, Tecnar Automation, Saint Bruno, Que., Canada). The diagnostic tool is based on optical pyrometry and time-of-flight measurements to measure the distribution of particle temperature and velocity in the thermal spray jet. The parameter sets that produced similar distributions of particle temperature and velocity in the thermal spray jet for both feedstock particles were selected for coating production. A total of 5000 particles for each feedstock were measured at the centerline of the thermal spray jet, where the particle flow density was the highest. The particle detector was placed at the same spray distance as used when depositing the coatings, i.e., 20 cm from the torch nozzle.

During the spraying process a cooling system (air jets) was applied to reduce the coating temperature, which was monitored using a pyrometer. The maximum surface temperature for both coatings was approximately 260 °C.

2.3. Structure and phase characterization

The nanostructural and microstructural features of the feedstock particles and HVOF-sprayed coatings were evaluated via scanning electron microscopy (SEM). The cross-sections of the coatings for SEM analysis (and indentation) were cut with a diamond saw, vacuum impregnated with a low viscosity epoxy resin and polished to a mirror finish with diamond and alumina particles.

The porosity of the coatings was measured via image analysis and SEM. Ten images per coating were analyzed in order to determine the porosity levels. X-ray diffraction (XRD) (Cu Kα radiation) was used to determine the phases present in the coatings. A 2θ diffraction angle ranging from 20° to 80° (using a step size of 0.05° and step time of 2.5 s) was employed.

2.4. Microhardness and crack propagation resistance

Vickers microhardness measurements were performed under a 300 g load for 15 s on the cross-section of the coatings. A total of 10 microhardness measurements were carried out for each coating. The crack propagation resistance was determined by indenting the coating cross-section with a Vickers indenter at a 5 kg load for 15 s, with the indenter aligned such that one of its diagonals would be parallel to the substrate surface. The total length of the major crack ($2c$) parallel to the substrate surface that originated at or near the corners of the Vickers indentation impression was measured. Based on the indentation load (P) and $2c$, the crack propagation resistance was calculated according to the relation between load and crack length $P/c^{3/2}$ [21] where P is in Newtons and c is in meters. All indentation cracks were significantly larger than the diagonal length of the indentation impression ($2a$), i.e., $c \geq 2a$. Therefore it is assumed that these cracks had half-penny geometry [21]. All the indentations were performed very near the centerline of the cross-section and the average of five indentations was taken for crack propagation resistance calculations.

2.5. Abrasion resistance and bond strength

The abrasion resistance of the coatings was tested based on the ASTM standard G65-00 (procedure D – modified) [22], also known as the dry sand/rubber wheel test. In this test, a stationary coated sample was pressed against a rotating rubber-coated wheel (228.6 mm diameter; 200 rpm) with a force of 45 N. Silica sand (212–300 μm) was fed (300–400 g/min) between the coating and rubber wheel until the wheel traveled over the equivalent linear distance of 1436 m. Prior to being submitted to this test, the surfaces of the coatings were prepared by grinding with diamond wheels to produce a flat surface. Two samples were tested for each coating produced in this study. The volume of the material abraded away during the test was measured via optical profilometry. It is important to point out that the abrasion test was performed at room temperature. The typical coating thicknesses for this test were 530–580 μm.

The bond strength of the coatings was tested using the ASTM standard C 633-01 for determining the adhesion or cohesion strength of thermal spray coatings [23]. A total of five samples were tested for each of the two different coating

types produced in this study. The typical coating thicknesses for this test were 390–450 μm.

2.6. Surface of the wear scar

The wear scars formed in the coatings during the abrasion tests were analyzed via SEM in order to observe the differences in scar smoothness and to identify regions of plastic deformation and fracture. During SEM the samples were tilted at 50° in order to obtain a better perspective of the scar morphology. The arithmetic mean roughness value (R_a) of the wear scars was measured perpendicular to the abrasion direction to quantify the smoothness. The arithmetic mean roughness value is the average deviation of a surface profile from the centerline over the measuring length, defined by:

$$R_a = \frac{1}{L}\int_{x=0}^{x=L} |y(x)|\,dx \quad (4)$$

where y is the deviation of the surface profile from the centerline and L is the measuring length. A total of 10 roughness measurements were performed for each coating.

3. Results and discussion

3.1. In-flight particle characteristics

Fig. 1 shows the temperature and velocity distributions for the particles in the thermal spray jet for the two feedstock powders. It is possible to observe that the shapes of the distributions are similar, however, the distribution of velocity for the conventional feedstock is somewhat shifted to higher speeds. The average particle temperature and velocity for the nanostructured feedstock particles was 1814 ± 158 °C and 647 ± 101 m/s, respectively. The average particle temperature and velocity for the conventional feedstock particles was 1811 ± 177 °C and 751 ± 117 m/s. Both these average velocities are quite high and very typical of HVOF systems [24]. Although the average velocity for the conventional particles was approximately 15% higher than that of the nanostructured particles, the following sections will demonstrate that this higher average velocity did not translate into a significant difference in the microstructure or a significant improvement in the mechanical performance of the conventional coating.

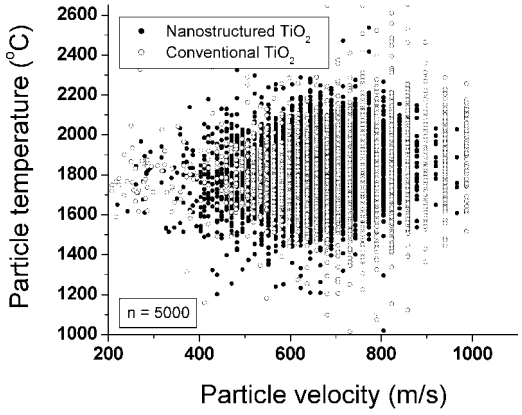

Fig. 1. Particle temperature and velocity distributions in the thermal spray jet for the nanostructured and conventional titania feedstock particles.

It is important to point out that the average particle temperature of the HVOF-sprayed nanostructured feedstock particles (1814 ± 158 °C) was close to the melting point of titania (1855 °C) [25]. This temperature distribution close to the melting point of titania will contribute to keeping intact part of the original nanostructure of the feedstock embedded in the coating microstructure, i.e., not all particles will be fully molten.

3.2. Feedstock particles

Fig. 2a shows a typical particle of the nanostructured titania feedstock. It exhibits the typical donut shape of spray-dried particles. When analyzed at high magnification it is possible to observe the nanostructure of the feedstock (Fig. 2b). Each microscopic feedstock particle is formed by agglom-

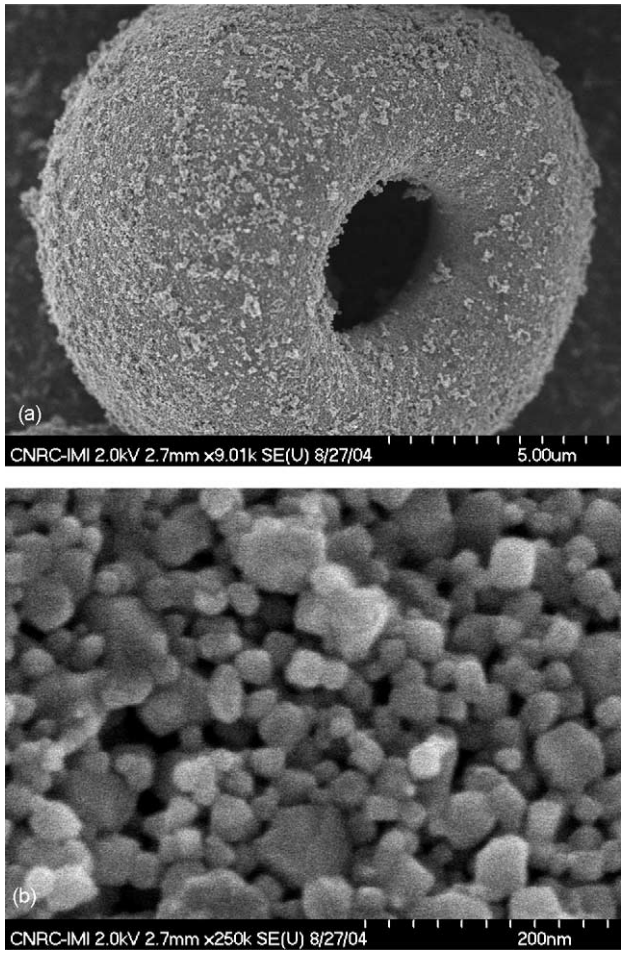

Fig. 2. (a) Titania feedstock particle formed by the agglomeration of individual nanosized particles of titania. (b) Particle of (a) observed at higher magnification; individual nanosized titania particles.

eration via spray-drying of innumerous individual nanosized particles of titania. All individual nanosized particles of titania are smaller than 100 nm. Therefore it is confirmed that this feedstock is nanostructured.

Fig. 3a shows a typical particle of the conventional titania feedstock. It exhibits flat surfaces and sharp edges regularly observed in fused and crushed particles. SEM at high magnification shows (Fig. 3b) that the particle is highly dense, not exhibiting nanostructural characteristics, which confirms the conventional character of this feedstock.

3.3. Bimodal and conventional coatings

Fig. 4 shows the cross-section of the titania coating made from the nanostructured feedstock. It is possible to observe that the coating microstructure is very uniform, not exhibiting the typical layered or lamellar structure of thermal spray coatings [26]. It may be stated that this coating has an isotropic microstructure. By looking at the microstructure of Fig. 4a at high magnification, a nanostructured zone is observed (Fig. 4b). The nanostructured zone is formed by a feedstock particle that was partially melted in the thermal spray jet. The nanostructured zone (Fig. 4b) is comprised of an agglomeration of individual nano-sized particles of titania with diameters less than 100 nm and it is possible to observe the similarities between this nanostructured zone and the nanostructured feedstock particle (Fig. 2b). The nanostructured zone is very well embedded in the conventional matrix formed by the feedstock particles that were fully molten in the thermal spray jet. The particles that were fully molten in the thermal spray jet lost their nanostructural character and therefore it is assumed that when they resolidify they will exhibit the same behavior as conventional thermally sprayed ceramic particles.

It is important to point out that the nanostructured zones like that of Fig. 4b are uniformly dispersed throughout the coating microstructure. Therefore it can be stated that the titania coatings made from the nanostructured feedstock exhibited a bimodal structure. This bimodal structure has also been observed by other authors who thermally sprayed nanostructured ceramic feedstock powders [15–19].

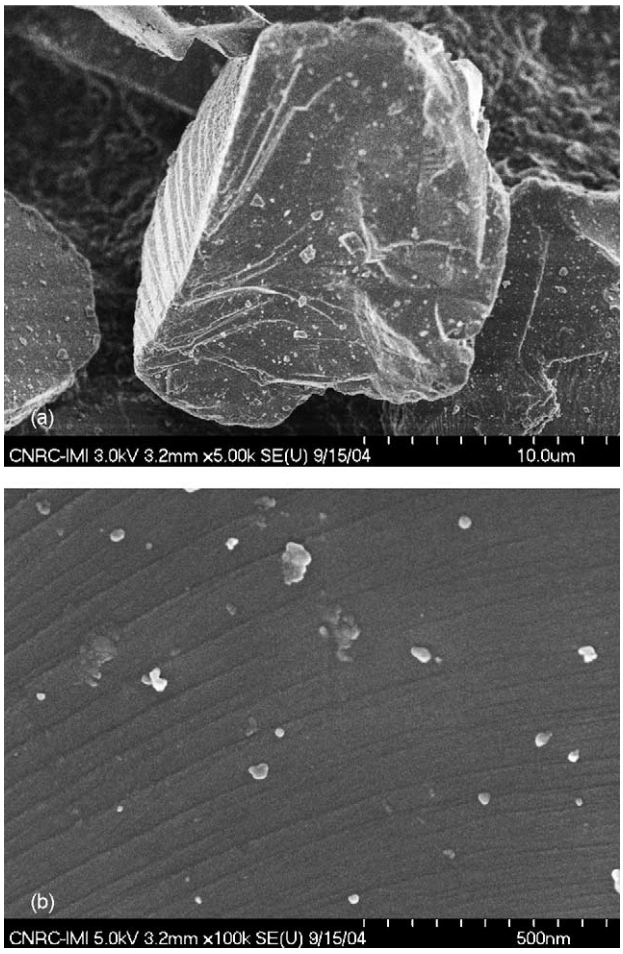

Fig. 3. (a) Conventional fused and crushed titania feedstock particle. (b) Particle of (a) observed at higher magnification; absence of nanostructural character.

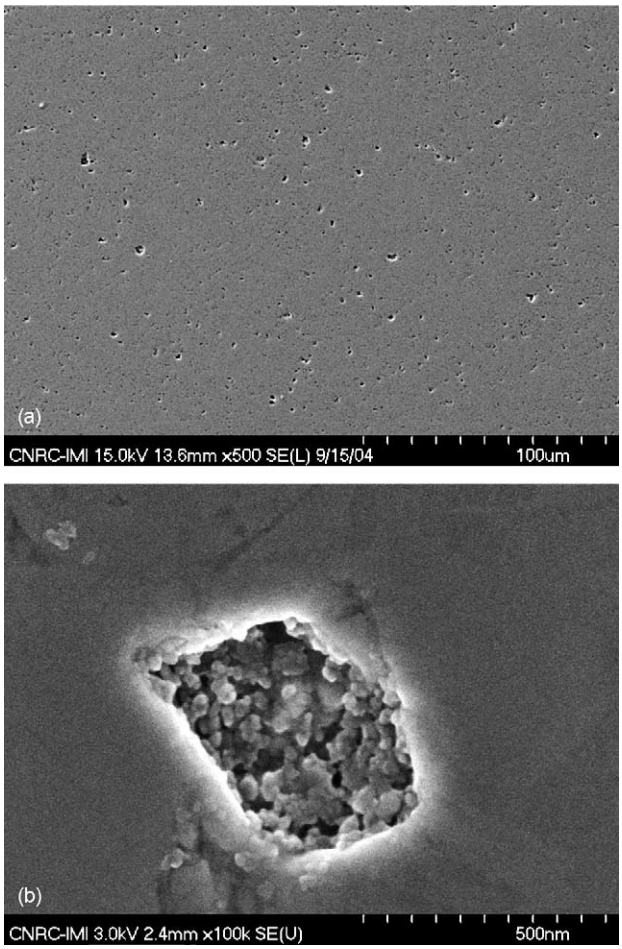

Fig. 4. (a) The cross-section of the titania coating made from the nanostructured feedstock. (b) Higher magnification view of (a) showing a nanostructured zone (formed by a particle that was semi-molten in the thermal spray jet) embedded in the conventional matrix (formed by particles that were fully molten in the thermal spray jet), i.e., bimodal structure.

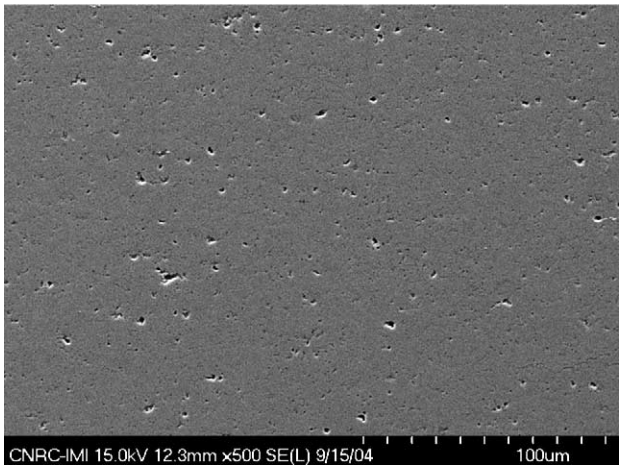

Fig. 5. The cross-section of the titania coating made from the conventional feedstock.

Fig. 5 shows the cross-section of the titania coating made from the conventional feedstock. This coating is also very uniform and isotropic-like, not exhibiting the typical layered or lamellar structure of thermal spray coatings [26]. The presence of semi-molten particles embedded in the coating microstructure is also possible, however, due to the character of the feedstock, the conventional characteristics of the coating will remain unchanged.

It is important to point out that the bimodal and conventional coatings are very dense, with porosity content less than 1% (Table 1). Therefore the objective of producing very dense coatings was achieved, and, as mentioned by others [11–14] and discussed in Section 1, dense microstructures are paramount when measuring or analyzing materials to determine meaningful ductility and toughness values and characteristics.

3.4. Phase content

Figs. 6 and 7 show the XRD patterns of the bimodal and conventional coatings, respectively. For both coatings, rutile is the major phase and anatase is the secondary phase. The conventional coating also seems to contain some amorphous titania. All the peaks of rutile and anatase observed in the bimodal coating are also observed in the conventional coating and vice-versa. Therefore it is considered that these two coatings exhibit similar phase content, which is very important in order to make a fair comparison of their mechanical performance and draw conclusions based on microstructural differences.

Table 1
Porosity, Vickers hardness and crack propagation resistance of the coatings made from the nanostructured and conventional titania feedstock powders

Coating	Porosity (%; $n = 10$)	Hardness (300 g; $n = 10$)	Crack propagation resistance (MPa $m^{1/2}$; $n = 5$)
Bimodal	<1	810 ± 26	28.4 ± 1.4
Conventional	<1	833 ± 30	17.2 ± 3.3

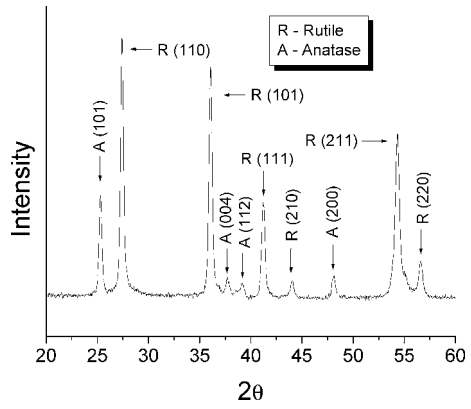

Fig. 6. XRD pattern of the coating made from the nanostructured feedstock (bimodal coating).

3.5. Hardness and crack propagation resistance

Vickers hardness and crack propagation resistance values for the two coatings can be found in Table 1. The two coatings exhibited very similar hardness values but the crack propagation resistance of the bimodal coating was 65% higher than that of the conventional coating. As both coatings are near pore-free (Table 1) and exhibit similar hardness (Table 1) and phase content (Figs. 6 and 7) it may be stated that the bimodal coating is tougher than the conventional coating, and this enhanced toughness appears to be a nanostructure-related property rather than a microstructural artifact.

Figs. 8 and 9 allow a visual comparison of the crack propagation resistance data of Table 1. The pictures show a Vickers indentation impression (5 kgf) performed on the cross-sections of the coatings. For both coatings, the horizontal cracks that originate at the corners of the Vickers indentation impression propagate parallel to the substrate surface. When the bimodal coating (Fig. 8) is compared to the conventional coating (Fig. 9), it is observed that the horizontal cracks of the conventional coating are more pronounced and longer than

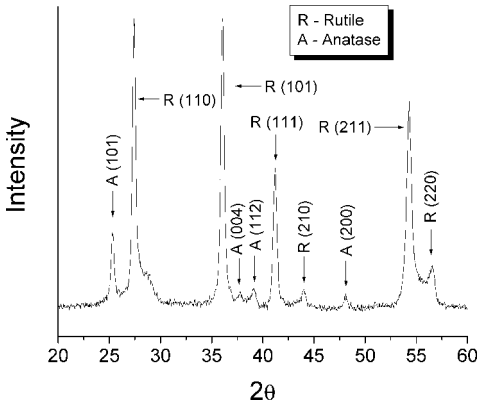

Fig. 7. XRD pattern of the coating made from the conventional feedstock.

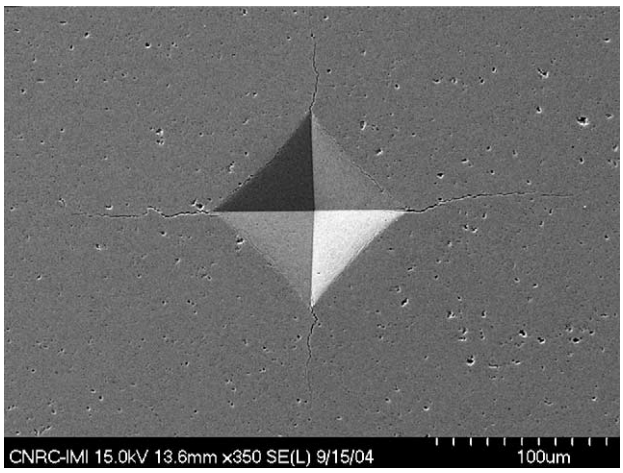

Fig. 8. Vickers indentation impression (5 kgf) and crack propagation in the cross-section of the titania coating made from the nanostructured feedstock (bimodal coating).

those of the bimodal coating. The bimodal coating exhibits shorter crack propagation under the same indentation load, therefore it is tougher. It is important to recall that two dense samples (porosity < 1%) of similar hardness are being compared. Consequently it is thought that this comparison is fair and meaningful.

The higher toughness of the bimodal coating is caused by the presence of the nanostructured zones embedded in the conventional matrix. It has been demonstrated that in bimodal coatings the nanostructured zones act as crack arresters [17,18,20,27]. In conventional thermally sprayed ceramic coatings, a crack will tend to propagate through the coating's weakest link, which is the well-defined layered structure, i.e., the splat or lamellar boundaries [28]. In bimodal coatings the splat or lamellar structure (i.e., the conventional matrix) is periodically disrupted by the nanostructured zones. Cracks propagating and reaching these well-embedded regions tend to be arrested by the nanostructured zones. Fig. 10 exemplifies how the crack arresting occurs in the bimodal coating. Fig. 10a shows a Vickers indentation crack being arrested by a nanostructured zone. Fig. 10b shows an example of a crack arresting near a nanostructured zone. The Vickers indentation crack loses its energy and is arrested by passing through the nanostructured zone. It is important to point out that as nanostructured zones are well embedded in the conventional ceramic matrix, the cracks do not skirt them.

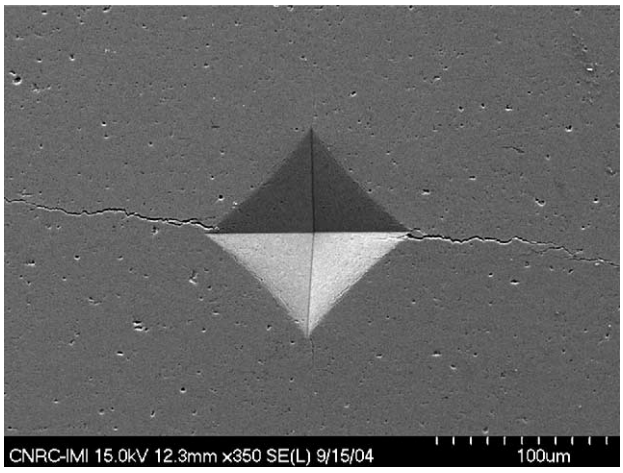

Fig. 9. Vickers indentation impression (5 kgf) and crack propagation in the cross-section of the titania coating made from the conventional feedstock.

Therefore based on the results of Table 1 and Figs. 8–10 it is observed that the bimodal coating is tougher than the conventional one without having to compromise its cohesive strength, i.e., hardness. The nanostructured zones in the bimodal structure do not promote an increase in hardness; instead, they act as crack arresters helping to impede crack propagation. As fracture toughness is also some measure of potential ductility [13], the higher toughness of the bimodal coating is the first indication in this study that it exhibits an enhanced ductility when compared to the conventional one.

It is interesting to point out that for the bimodal coating (Fig. 8) four cracks are observed originating at the corners of the Vickers indentation impression instead of just two. When Vickers indenting the cross-sections of ceramic thermal spray coatings at high loads (e.g., > 1 kgf), normally just two cracks propagate parallel to the substrate surface from the corners of the indentation impression [29]. The cracks tend to propagate parallel to the coating surface due to the weakest link offered by the layered structure of thermal spray coatings [28]. The high density, high homogeneity and isotropic character of the bimodal coating (characteristics not typical of thermal spray coatings [26]) may have contributed to the propagation of four cracks, similar to what would be found when Vickers indenting an isotropic bulk ceramic material [21]. The conventional titania coating also had a high density and high homogeneity, however, no isotropic crack propagation was observed during Vickers indentation. This difference in behavior of these two coatings may lie in the bimodal character of the coating made from the nanostructured feedstock. Further research is necessary in order to better understand and explain the role of this bimodal character.

One may argue that crack arresting could be caused by the presence of pores/micropores in the very dense HVOF microstructure, rather than by the embedded nanozones. It is known (via mercury intrusion porosimetry (MIP) measurements) that thermal spray coatings exhibit two types of porosity: (i) coarse porosity (3–10 μm) associated with defects in the structure due to the incomplete filling of interstices between previously deposited particles and (ii) fine pores in between splats (0.1 μm), which are an inherent feature of the coatings [28]. During HVOF spraying the coarse porosity is almost totally eliminated due to the high impact velocity of the sprayed particles (Fig. 1). However, the fine pores in between splats are present because they are inherent to the thermal spray coatings, i.e., both bimodal and conventional coatings exhibit this type of porosity. As both feedstock powders (nanostructured and conventional) exhibited similar particle size distributions and similar distributions of particle tem-

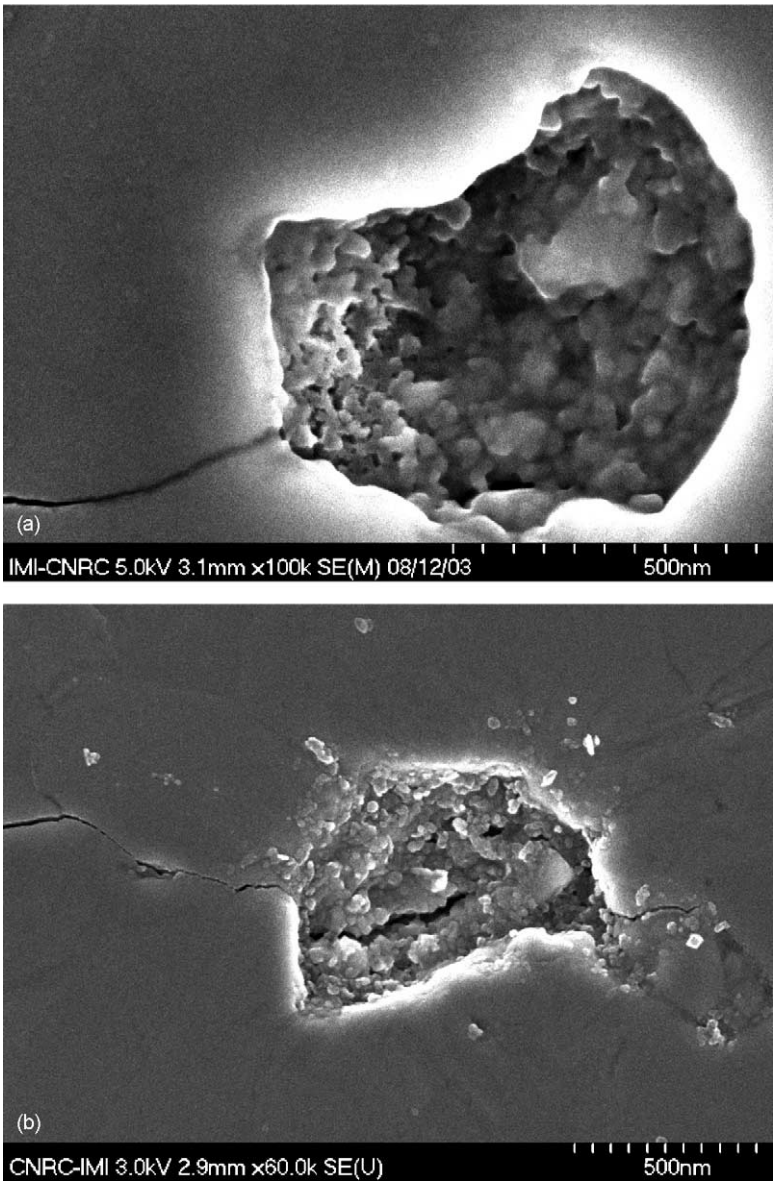

Fig. 10. (a) Vickers indentation crack being arrested by a nanostructured zone in the bimodal coating [20]. (b) Vickers indentation crack being arrested by passing through a nanostructured zone in the bimodal coating [27].

perature and velocity in the spray jet (Fig. 1), it seems to be correct to expect that their respective coatings exhibit similar levels, distributions and forms of porosity. Consequently, if porosity were causing a crack arresting effect it would be observed for both coatings, not only for the bimodal one. It is important to point out that these two coatings were produced under very similar conditions in order to pinpoint real nanostructural effects.

In addition to this explanation it is important to point out that processes like HVOF, vacuum plasma spray (VPS) and detonation gun (D-Gun) are used to produce thermal spray coatings with minimum porosity levels in order to increase their mechanical strength. No references have been identified by the author claiming that pores may arrest cracks in thermal spray coatings, however, according to Gell et al. [17] and Luo et al. [18], it has been demonstrated that the semi-molten zones (nanozones) arrest cracks in thermal spray coatings, i.e., these references agree with the experimental observations of this study.

3.6. Wear resistance and bond strength

Table 2 shows the results of abrasion resistance (in terms of volume loss) and bond strength for the bimodal and conventional titania coatings. The bimodal coating exhibits a 25% lower average volume loss and an average bond strength that is 2.4 times higher when compared to the conventional coating. Due to the similarities in particle temperature–velocity distributions, porosity levels and phase content of the two coatings, the higher abrasion resistance of the bimodal coat-

ing is explained by its higher toughness (without compromising its hardness, as discussed in the previous section).

The higher bond strength of the bimodal coating may be explained by the higher interfacial toughness of thermal sprayed ceramic coatings made from nanostructured feedstock powders [30]. Bansal et al. [30] compared the interfacial toughness of bimodal and conventional air plasma sprayed Al_2O_3–13wt.% TiO_2 coatings. For the conventional coating it was observed that the interfaces between the particles that were fully molten in the thermal spray jet and the steel substrate exhibited microcracks. For the bimodal coating it was observed that the interfaces between the particles that were semi-molten in the thermal spray jet (nanostructured zones) and the steel substrate were adherent, i.e., no microcracks. Therefore an interfacial crack in the bimodal coating would be interrupted by the strong adherent nanostructured zones, thereby increasing interfacial toughness and bond strength [30]. This phenomenon is somewhat similar to that observed in Fig. 10.

3.7. Plasticity of the wear scar of the bimodal coating

Fig. 11 shows the morphology of the wear scar of the bimodal coating. It is observed that the majority of the material removal occurred without significant cracking, fragmentation or scratching. In fact the surface looks predominantly smeared and dulled, which is a typical characteristic of plastic deformation.

On the other hand, the morphology of the wear scar of the conventional coating shows different characteristics (Fig. 12). The surface is rougher when compared to that of the bimodal coating (Fig. 11). Some plastic deformation is observed (smeared zones), however, scratches and fragmentation occupy a significant area of the wear scar. A considerable amount of material is removed in large amounts due to the lack of ductility of the coating, forming "canyons" on the surface of the scar. In these "canyons" it is possible to observe fragments that are barely attached to the scar surface (Fig. 12b), which after subsequent wear will be easily removed from the coating surface, thereby increasing the volume loss.

It has been shown that plastic deformation (i.e., ductile flow) and fragmentation (i.e., brittle fracture) occur during grinding of thermal spray ceramic coatings [31]. During the grinding of a ceramic material, a transition of material removal mechanism from ductile mode to brittle mode occurs. The initial ductile flow progressively changes to brittle fracture after a critical depth of cut is reached. The critical depth of cut of a ceramic material is directly proportional to its toughness-to-hardness ratio [31]. Therefore the bimodal coating, which exhibited almost the same hardness and 65% higher crack propagation resistance (i.e., higher toughness) when compared to the conventional coating (Table 1) should also exhibit a higher critical depth of cut. This higher critical depth of cut (i.e., large region for plastic deformation) should translate into a smoother wear scar, as observed in Fig. 11. Due to the lower critical depth of cut of the conventional coating (i.e., small region for plastic deformation), the transition of material removal from ductile mode to brittle mode is more prone to occur. Consequently, more irregularities, scratches and fragmentation are observed on the scar surface of the conventional coating (Fig. 12).

The roughness values (R_a) of the wear scars of the bimodal and conventional coatings are 0.06 ± 0.02 and 0.08 ± 0.02 μm, respectively. A total of 10 roughness measurements were performed for each coating and the analysis

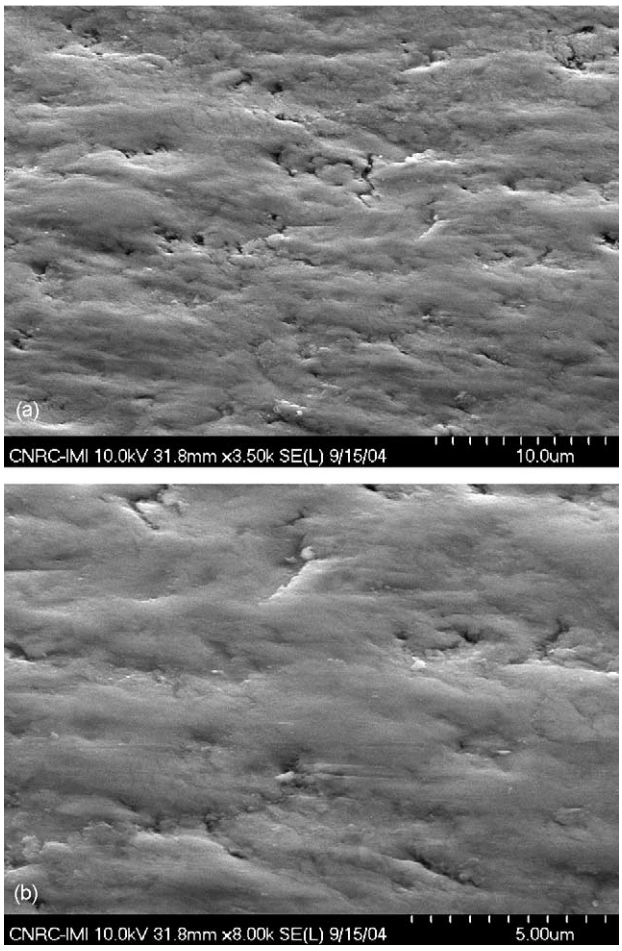

Fig. 11. (a) SEM picture (taken at 50°) of the wear scar of the bimodal coating. (b) Higher magnification view of (a) showing the predominant ductile deformation of the bimodal coating during abrasive wear.

Table 2
Abrasion resistance (in terms of volume loss) and bond strength of the coatings made from the nanostructured and conventional titania feedstock powders

Coating	Volume loss (mm^3; $n = 2$)	Bond strength (MPa; $n = 5$)
Bimodal	14.7 ± 0.2	56 ± 22
Conventional	19.7 ± 1.1	23 ± 5

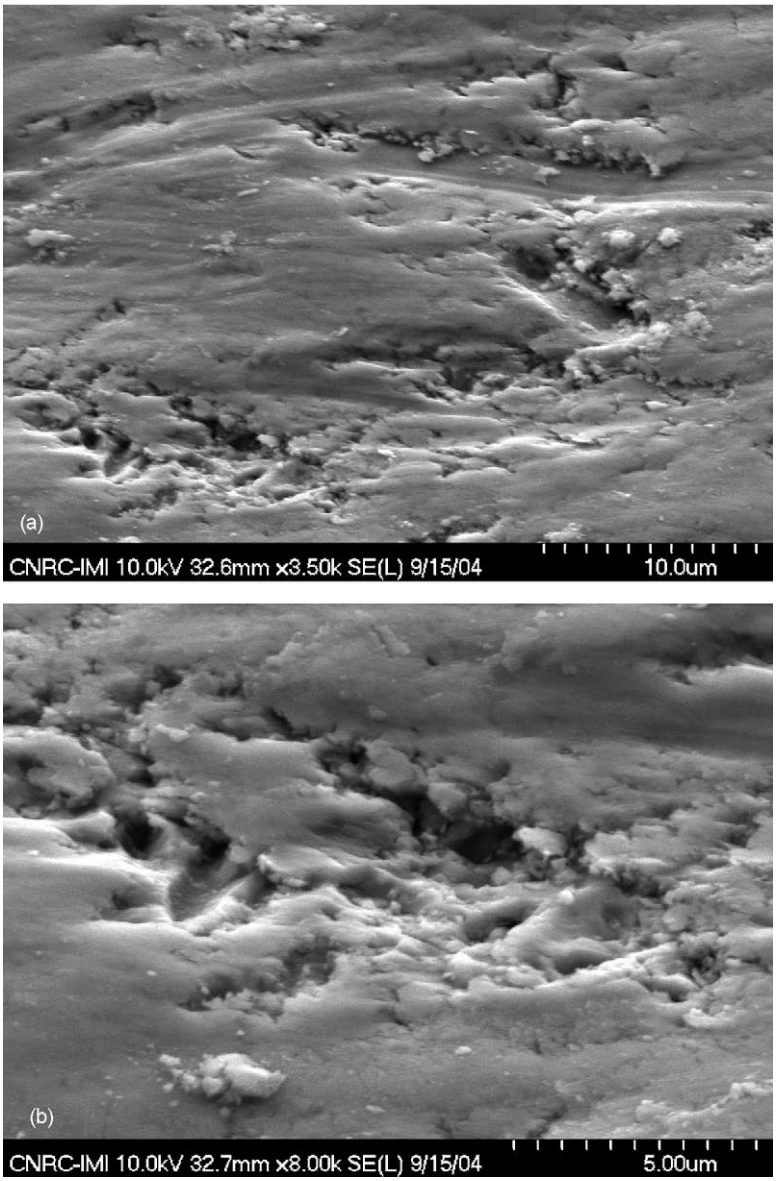

Fig. 12. (a) SEM picture (taken at 50°) of the wear scar of the conventional coating. (b) Higher magnification view of (a) showing the typical fracture characteristics of the conventional coating during abrasive wear.

of variance (ANOVA) demonstrated that there is a statistically significant difference between the means of the two roughness values at the 95% confidence level. This decrease of 25% in average roughness of the bimodal coating agrees with the morphological characteristics observed in Figs. 11 and 12, i.e., the surface of the wear scar of the bimodal coating is less rough. Therefore the results of crack propagation resistance (Table 1), the morphological characteristics of the wear scars (Figs. 11 and 12) and the roughness measurements reinforce the claim that the bimodal coating exhibits enhanced ductility at low temperatures (well below $0.5T_m$). This enhanced ductility should allow more energy absorption during abrasive wear, thereby helping to produce lower volume loss as observed in this work (Table 2).

3.8. Engineering considerations

Titania thermal spray coatings are usually employed in anti-wear applications [19]. The higher abrasion resistance and the higher bond strength of the bimodal coating are obvious advantages for the replacement of the conventional coating. However, the enhanced ductility exhibited by the bimodal coating is also an important advantage because it probably increases the machinability of the coating. As-sprayed coatings are rarely ready for use. In most practical applications (mainly in wear), the as-sprayed coatings have to be ground and polished to arrive at the dimensions that fall within the specified range and to produce the required coating roughness [26,32]. This process can be expensive and time-consuming,

therefore, employing a highly machinable coating may significantly reduce the cost of a component.

4. Conclusions

- During this work HVOF-sprayed titania coatings were produced from nanostructured and conventional feedstock powders. The goal of producing coatings with similar distributions of particle temperature–velocity in the thermal spray jet, near pore-free, isotropic-like microstructures, and similar phase content was realized. Achieving these characteristics was very important for producing meaningful and non-biased results for comparisons of mechanical performance.
- The coating made from the nanostructured feedstock exhibited a bimodal structure, where particles that were semi-molten in the thermal spray jet (nanostructured zones) were well embedded in a matrix of the particles that were fully molten in the thermal spray jet (conventional matrix).
- The nanostructured zones in the bimodal coating were uniformly dispersed throughout the coating microstructure.
- Both coatings exhibited almost the same Vickers hardness, however, the crack propagation resistance of the bimodal coating was 65% higher than that of the conventional coating. Therefore it may be stated that the bimodal coating was tougher than the conventional one. It is important to point out that the cohesive strength (i.e., hardness) of the bimodal coating did not have to be compromised in order to gain toughness. This is a nanostructure-related characteristic.
- The higher crack propagation resistance or toughness of the bimodal coating was attributed to the nanostructured zones that were well embedded in the coating microstructure (conventional matrix) and act as crack arresters helping to impede crack propagation.
- The bimodal coating exhibited a 25% lower average volume loss during abrasion tests when compared to the conventional coating. The lower volume loss is probably explained by the higher toughness of the bimodal coating.
- The bimodal coating exhibited an average bond strength 2.4 times higher when compared to the conventional coating. This higher bond strength may be explained by the presence of the well-adhered nanostructured zones in the coating/substrate interface. These strongly adhering nanostructured zones would serve to interrupt the propagation of an interfacial crack in the bimodal coating [30].
- Scanning electron microscopy observations showed that the wear scar surface morphology of the bimodal coating had fewer protuberances (more leveled) and exhibited typical characteristics of ductility and plastic deformation, whereas, the conventional coating exhibited scratches and fragmented regions (canyons) that were probably caused by its lack of ductility.
- The smoother wear scar of the bimodal coating (25% lower average roughness R_a) was probably given by its higher critical depth of cut, which provided a broader plastic deformation range than that exhibited by the conventional coating.
- The results of crack propagation resistance and the smoothness of the wear scar (observed by SEM and roughness measurements) indicated that the bimodal coating exhibited enhanced ductility when compared to the conventional coating. As both coatings were produced under similar conditions it is thought that this enhanced ductility at low temperature (well below $0.5T_m$) of the bimodal coating is strong evidence of a nanostructure-related property of the ceramic material (i.e., not caused by any other microstructural artifact), a characteristic that is being sought by researchers working on nanostructured materials.

Acknowledgements

Part of the results of this paper originated from research funded by Altair Nanomaterials Inc. (Reno, NV, USA). The authors thank Altair Nanomaterials Inc. for encouraging the publication of these results. The authors also thank F. Belval for HVOF spraying, M. Lamontagne for the DPV2000 measurements, E. Poirier for metallography and M. Thibodeau for SEM pictures and XRD patterns.

References

[1] H. Gleiter, Acta Mater. 48 (1999) 1–19.
[2] Y. Lu, P.K. Liaw, J. Met. (2001) 31–35, March.
[3] M.J. Mayo, NanoStruct. Mater. 9 (1997) 717–726.
[4] A.J.A. Winnbust, M.M.R. Boutz, Y.J. He, A.J. Burggraaf, H. Verweij, Ceram. Int. 23 (1997) 215–221.
[5] Y.T. Zhu, X. Liao, Nature Mater. 3 (2004) 351–352, June.
[6] R. Valiev, Nature Mater. 3 (2004) 511–516, August.
[7] K.J. Hemker, Science 304 (9) (2004) 221–223, April.
[8] S. Yip, Nature Mater. 3 (2004) 11–12, January.
[9] Y. Wang, M. Chen, F. Zhou, E. Ma, Nature 419 (2002) 912–915.
[10] M.J. Mayo, R.W. Siegel, A. Narayanasamy, W.D. Nix, J. Mater. Res. 5 (5) (1990) 1073–1082, May.
[11] B.A. Cottom, M.J. Mayo, Scripta Mater. 34 (5) (1996) 809–814.
[12] F. Tancret, F. Osterstock, Phil. Mag. 83 (1) (2003) 125–136.
[13] C.C. Koch, D.G. Morris, K. Lu, A. Inoue, MRS Bull. (1999) 54–58, February.
[14] M.J. Mayo, NanoStruct. Mater. 9 (1997) 717–726.
[15] R.S. Lima, A. Kucuk, C.C. Berndt, Mater. Sci. Eng. A 313 (2001) 75–82.
[16] R.S. Lima, A. Kucuk, C.C. Berndt, Mater. Sci. Eng. A 327 (2002) 224–232.
[17] M. Gell, E.H. Jordan, Y.H. Sohn, D. Goberman, L. Shaw, T.D. Xiao, Surf. Coat. Technol. 146–147 (2001) 48–54.
[18] H. Luo, D. Goberman, L. Shaw, M. Gell, Mater. Sci. Eng. A 346 (2003) 237–245.
[19] G.E. Kim, J. Walker Jr., J.B. Williams Jr., US Patent 2003/0049449 A1, March 13, 2003.
[20] R.S. Lima, B.R. Marple, Surf. Coat. Technol., accepted for publication.
[21] G.R. Anstis, P. Chantikul, B.R. Lawn, D.B. Marshall, J. Am. Ceram. Soc. 64 (9) (1981) 533.
[22] Standard Test Method for Measuring Abrasion Using the Dry Sand/Rubber Wheel Apparatus, ASTM Standard G65-00. ASTM, West Conshohocken, PA, USA.

[23] Standard Test Method for Adhesion or Cohesion Strength of Thermal Spray Coatings, ASTM Standard C 633-01. ASTM, West Conshohocken, PA, USA.
[24] B.R. Marple, R.S. Lima, in: B.R. Marple, C. Moreau (Eds.), Thermal Spray 2003: Advancing the Science and Applying the Technology, ASM International, Materials Park, OH, USA, 2003, pp. 273–282.
[25] M. Miyayama, K. Koumoto, H. Yanagida, in: S.J. Schneider (Ed.), Engineered Materials Handbook, Ceramic and Glasses, vol. 4, ASM International, Materials Park, OH, USA, 1991, pp. 748–757.
[26] L. Pawlowski, The Science and Engineering of Thermal Spray Coatings, Wiley, West Sussex, England, 1995.
[27] R.S. Lima, B.R. Marple, J. Thermal Spray Technol., submitted for publication.
[28] R. McPherson, Surf. Coat. Technol. 39/40 (1989) 173–181.
[29] P. Ostojic, R. McPherson, Mater. Forum 10 (4) (1987) 247–255.
[30] P. Bansal, N.P. Padture, A. Vasiliev, Acta Mater. 51 (2003) 2959–2970.
[31] X. Liu, B. Zhang, Z. Deng, Int. J. Machine Tools Manuf. 42 (2002) 1665–1676.
[32] R.C. Tucker Jr., in: C.M. Cotell, J.A. Sprague, F.A. Smidt Jr. (Eds.), ASM. Handbook, Surface Engineering, 5, ASM International, Materials Park, OH, USA, 1994, pp. 497–509.